

LDN Protects Bone Property Deterioration at Different Hierarchical Levels in T2DM Mice Bone

Pankaj Shitole, Abhinav Choubey, Prosenjit Mondal,* and Rajesh Ghosh*

Cite This: *ACS Omega* 2021, 6, 20369–20378

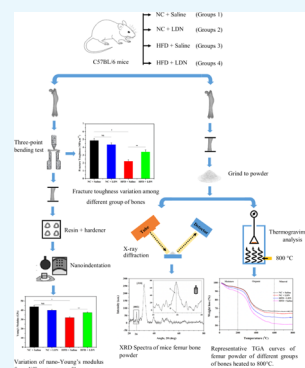
Read Online

ACCESS |

Metrics & More

Article Recommendations

ABSTRACT: Type 2 diabetes mellitus (T2DM) commonly affects bone quality at different hierarchical levels and leads to an increase in the risk of bone fracture. Earlier, some anti-diabetic drugs showed positive effects on bone mechanical properties. Recently, we have investigated that low-dose naltrexone (LDN), a TLR4 antagonist treatment, improves glucose tolerance in high-fat diet (HFD)-induced T2DM mice and also gives protection against HFD-induced weight gain. However, effects on bone are still unknown. In this study, the effects of LDN on the bone properties at different hierarchical levels in T2DM mice bone were investigated. In order to investigate these, four different groups of bone (divided based on diet and treatment) were considered in this present study. These are (a) normal control diet treated with saline water, (b) normal control diet treated with LDN, (c) HFD treated with saline water, and (d) HFD treated with LDN. Bone properties were measured in terms of fracture toughness, nano-Young's modulus, hardness, mineral crystal size, bone composition, and bulk mineral to matrix ratio. Results indicated that fracture toughness, nano-Young's modulus, and hardness were decreased in T2DM bone as compared to normal bone, and interestingly, treatment with the LDN increases these material properties in T2DM mice bone. Similarly, as compared to the normal bone, decrease in the mineral crystal size and bulk mineral-to-matrix ratio was observed in the T2DM bone, whereas LDN treatment protects these alterations in the T2DM mice bone. The bone size (bone geometry) was increased in the case of HFD-induced T2DM bone; however, LDN cannot protect to increase the bone size in the T2DM mice bone. In conclusion, LDN can be used to control the T2DM-affected bone properties at different hierarchical levels.



1. INTRODUCTION

High-fat diet (HFD) is known to induce basal hyperinsulinemia and promote type 2 diabetes mellitus (T2DM).¹ In the case of T2DM condition, bone is prone to fracture; however, the bone mineral density is not affected or even higher in diabetic patients.² The incidence of diabetes and obesity has extended epidemic status in the world; as estimated by International Diabetes Federation, there are approximately 422 million persons with T2DM in the world, and as forecast by the World Health Organization, it is expected that the number might reach 600 million by 2030.³ T2DM is a progressive condition in which the body becomes insulin-resistant; therefore, the level of blood sugar rises to higher than normal. However, several anti-diabetic compounds are widely used to control blood sugar levels.⁴ It has been observed that T2DM impacts bone structural and mechanical properties in mice bone.⁵ Recently, low-dose naltrexone (LDN) exhibited enhanced glucose tolerance and insulin sensitivity in HFD-induced T2DM mice.⁶ Although naltrexone was synthesized as an orally active competitive opioid receptor antagonist, LDN exhibits paradoxical properties, including analgesia and anti-inflammatory actions, where LDN simultaneously has an antagonist effect on nonopioid receptors (TLR4) which have not been reported at larger dosages.^{7–9} Recently, we have identified that LDN can control Raman-based compositional

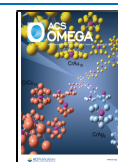
bone quality parameters in T2DM mice bone.¹⁰ However, the influence of LDN on T2DM-affected bone properties in terms of fracture toughness, nano-Young's modulus, hardness, mineral crystal size, and bone composition is still unknown.

Several studies indicated that obesity leads to increased bone density, bone geometric properties, and fracture risk in mice and adults.^{5,11–13} Obesity can be related to microstructural and mechanical behavior changes in bone.¹⁴ In general, due to T2DM, the bone quality is reduced with an increase in bone quantity (higher bone mass and higher geometric parameters) to explain the altered fracture risk. Earlier studies have addressed the reduced size-independent mechanical properties despite larger bone sizes in HFD-induced T2DM bones.^{5,15} The interpretation of mechanical and structural properties at multiple length scales is necessary for the understanding of bone toughening mechanisms.^{16–18} At the whole-bone level (macro-scale), cortical bone is the compact one while, at the

Received: May 6, 2021

Accepted: July 19, 2021

Published: July 28, 2021



tissue level (micro-scale), lamellar bone is built up of collagen fibers, which are composed of collagen fibrils and mineral crystals (nano-scale). The hierarchical structure of the bone includes apatite mineral, impure forms of hydroxyapatite (HA), organic matter, composed of collagen and non-collagenous proteins, and water molecules. Because of this complex structure at different scale levels, there are many determinants of bone properties. At the nano-scale, mineral and collagen, as well as the interaction between them, contribute to bone-toughening mechanisms.^{19,20} Even though collagen plays a crucial role in bone toughness,^{19,20} it is also noted that bone mineral is altered due to disorders.²¹

X-ray diffraction (XRD) analysis has been extensively employed in the study of bone mineralized tissue, especially in the measurement of bone mineral crystal size.^{22,23} de Jong²⁴ was first to use XRD of bone and establish the mineral phase of bone tissue as HA. Additionally, this analysis also plays an important role in interpreting the structure of the principal protein component of bone and collagen.²² It was mentioned in the literature about the changes in bone mineral crystallinity with age and has been measured in several species, including humans, mice, rabbit, and chicken.^{24,25} The bone mechanical properties depend upon the mineral crystal size; hence, investigators have been interested in the measurement of bone mineral crystal size. In the case of brittle bone disease, such as osteogenesis imperfecta (*oim*^{-/-}), mineral crystal size had reduced due to the damaged collagen fibril template.²³ Additionally, thermogravimetric analysis (TGA) has been used to assess the influence of heat degradation on the individual constituents of bone.^{23,26} It was noted that in *oim*^{-/-} disease, bulk bone mineral content was reduced, which resulted in a decrease in the mineral to matrix ratio as compared with the normal bone.²³ The probable reason is an increase in the total organic fraction in the pathologic bone which is associated with collagen alteration.²³

A number of anti-diabetic drugs are used to control high blood sugar (for T2DM patients). Recently, LDN showed enhanced glucose tolerance and insulin sensitivity in T2DM mice.⁶ A recent study showed that naltrexone treatment increases the bone strength and energy absorbed in type 1 diabetic bone.²⁷ Similarly, some other studies also indicated the positive effect of naltrexone on bone mass^{28,29} and bone formation²⁹ and prevent bone loss.³⁰ We have also identified that LDN can control Raman-based compositional bone quality parameters in T2DM mice bone.¹⁰ However, to the author's knowledge, there is a dearth of an in-depth study to understand the effect of T2DM and LDN compound on bone properties such as fracture toughness, nano-properties, bone mineral crystal size, and bone composition. It has been anticipated that T2DM and LDN compounds might have an influence on bone properties at macro to nano level. In this study, C57BL/6 mice were chosen and fed on HFD to develop a diet-induced T2DM model which replicates the moderate to severe condition of diabetes in human beings. One group of HFD mice were treated with LDN compound. The objective of this study was to understand the effects of T2DM and LDN on bone fracture toughness, nano-Young's modulus, hardness, apatite mineral crystal size, and mineral properties.

2. RESULTS

2.1. Fracture Toughness: LDN Increases Fracture Toughness in HFD-Induced T2DM Mice. The fracture toughness of group 1, group 2, group 3, and group 4 bones was

found to be 4.86 (± 0.24), 4.34 (± 0.2), 2.21 (± 0.19), and 3.41 (± 0.26) MPa m^{1/2}, respectively (Figure 1). A two-ways

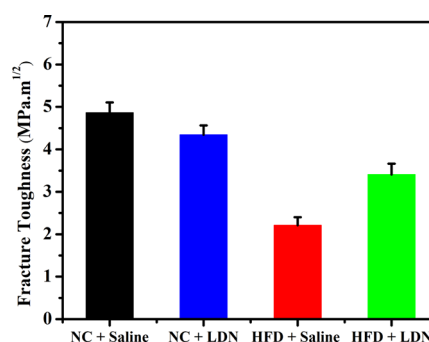


Figure 1. Fracture toughness of different groups of bones. Two-way ANOVA results indicated a significant effect of diet ($F_{1,20} = 360.12$, $p < 0.001$) on fracture toughness, similarly a significant interaction between effects of diet and treatment was observed ($F_{1,20} = 84.58$, $p < 0.001$); Bonferroni's post-hoc results indicated no significant difference between group 1 and group 2 ($p > 0.05$), whereas a significant difference between group 1 and other two groups was observed ($p < 0.05$). $n = 6/\text{group}$.

ANOVA test indicated that the diet have significant influence on fracture toughness ($p < 0.05$). It is interesting to note that there was statistical significant interactions between the effects of diet, and treatment on fracture toughness was observed ($p < 0.05$).

2.2. Bone Size: LDN Unable to Restore HFD-Induced Increased Bone Size. Mean and standard deviation of bone geometric parameters of four groups of bones are presented in Figure 2. In comparison to group 1 bone (normal bone), bone geometric parameters were increased for group 3 bones and group 4 bones (Figure 2). Overall, statistical analysis indicated significant influence of diet on bone size ($p < 0.05$) and no significant influence of treatment on bone size ($p > 0.05$). No statistical significant interaction between the effects of diet and treatment on bone size was observed ($p > 0.05$). These results suggested that bone size was increased for HFD bones, as compared to normal bones. However, LDN cannot protect to increase the bone size in the T2DM mice group (Figure 2).

2.3. Nano-Young's Modulus and Hardness: LDN Increases Young's Modulus and Hardness in HFD-Induced T2DM Mice. Local Young's modulus and hardness for four different groups of (group 1–4) bones are indicated in Figure 3a,b. The mean (\pm standard deviation) value of Young's modulus of group 1, group 2, group 3, and group 4 bone was found to be 40.62 (± 1.51), 38.01 (± 0.83), 29.05 (± 0.88), and 34.37 (± 0.75) GPa, respectively (Figure 3a). The mean (\pm standard deviation) value of hardness of group 1, group 2, group 3, and group 4 bone was found to be 1.91 (± 0.124), 1.71 (± 0.082), 1.02 (± 0.14), and 1.41 (± 0.073) GPa, respectively (Figure 3b). A two-way ANOVA test indicated that diet has significant influence on Young's modulus and hardness values ($p < 0.05$). Similarly, statistical significant interaction between the effects of diet and treatment on Young's modulus and hardness were observed ($p < 0.05$). The present study indicated that HFD would deteriorate the bone Young's modulus and hardness, whereas the LDN compound can resist deteriorating the bone Young's modulus and hardness.

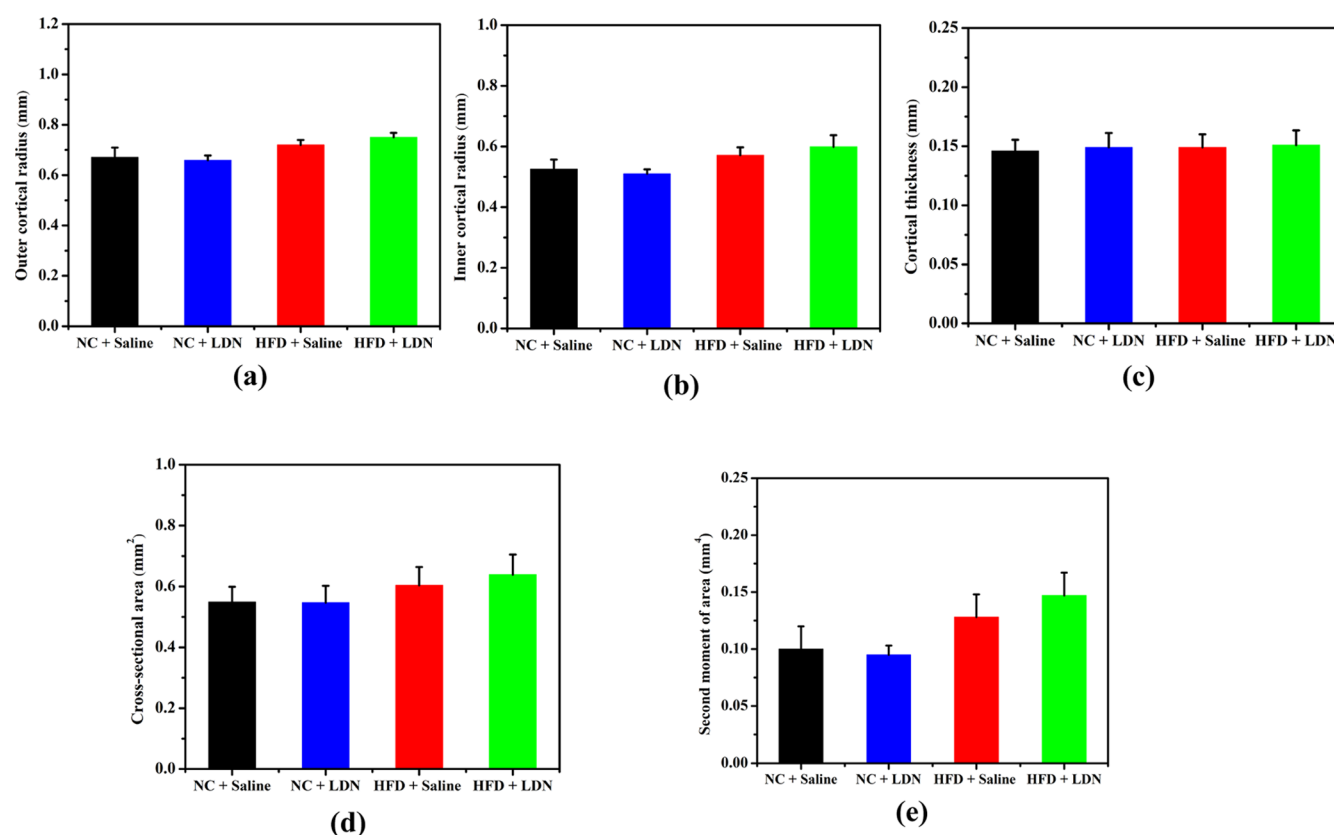


Figure 2. Bone size of different groups of bones; (a) outer cortical radius. Two-way ANOVA results showed a significant effect of diet ($F_{1,20} = 59.47$, $p < 0.001$) on outer cortical radius, similarly a significant interaction between effects of diet and treatment ($F_{1,20} = 5.29$, $p = 0.032$) was observed, results from Bonferroni's post-hoc test showed no significant difference between group 1 and group 2 bones ($p > 0.05$), whereas a significant difference between group 1 and other two groups ($p < 0.05$) was observed; however, $p > 0.05$ between group 3 and group 4 was observed; (b) inner cortical radius. Two-way ANOVA results indicated a significant effect of diet ($F_{1,20} = 32.05$, $p < 0.001$) on cortical inner radius, whereas no significant interaction between effects of diet and treatment ($F_{1,20} = 3.32$, $p = 0.083$) was observed, Bonferroni's post-hoc test showed no significant difference between group 1 and group 2 ($p > 0.05$), whereas a significant difference between group 1 and other two groups ($p < 0.05$) was observed; however, $p > 0.05$ between group 3 and group 4 was observed; (c) cortical thickness. Two-way ANOVA results showed no significant effect of diet ($F_{1,20} = 0.288$, $p = 0.597$) and no significant interaction between effects of diet and treatment ($F_{1,20} = 0.012$, $p = 0.916$), results from Bonferroni's post-hoc test showed no significant difference between group 1 and other groups ($p > 0.05$); (d) cross-sectional area. Two-way ANOVA results indicated a significant difference between the effect of diet ($F_{1,20} = 9.35$, $p < 0.01$) and interaction between effects of diet and treatment ($F_{1,20} = 0.57$, $p = 0.459$), Bonferroni's post-hoc result showed no significant difference between group 1 and other groups ($p > 0.05$); and (e) second moment of inertia. Two-way ANOVA results indicated a significant effect of diet ($F_{1,20} = 20.42$, $p < 0.001$) and no significant interaction between effects of diet and treatment ($F_{1,20} = 2.01$, $p = 0.172$), Bonferroni's post-hoc test showed $p > 0.05$ between group 1, group 2, and group 3, Bonferroni's post-hoc test showed a significant difference between group 1 and group 4 ($p < 0.05$), no significant difference between group 2 and group 3 ($p > 0.05$), and similarly no significant between group 3 and group 4 ($p > 0.05$). $n = 6/\text{group}$.

2.4. Mineral Crystal Size: LDN Increases the Mineral Crystal Size in HFD-Induced T2DM Mice. For group 1, group 2, group 3, and group 4 bone, the mineral crystal size was found to be $22.3 (\pm 0.96)$, $21.6 (\pm 0.81)$, $7.2 (\pm 0.64)$, and $14.47 (\pm 0.8)$ nm, respectively (Figure 4). Statistical analysis indicated that the diet has significant influence on mineral crystal size ($p < 0.05$). In this case also, statistically significant interaction between the effects of diet and treatment on mineral crystal size were observed ($p < 0.05$). These data indicated that in T2DM conditions, mineral crystal size is decreasing, as compared to the normal bone, while LDN treatment protects this alteration in the T2DM mice group (Figure 4).

2.5. Bulk Mineral-to-Matrix Ratio and Mineral Content: LDN Increases Mineral-to-Matrix Ratio and Mineral Content in HFD-Induced T2DM Mice. The percentages of weight-related with organic content [$m_{200^\circ\text{C}}(\%) - m_{600^\circ\text{C}}(\%)$], mineral content [$m_{600^\circ\text{C}}(\%)$], and

carbonate content [$m_{600^\circ\text{C}}(\%) - m_{800^\circ\text{C}}(\%)$] are shown in Table 1. The weight loss related to moisture was ignored because it might have been affected during sample preparation. The mineral content was reduced for group 3 bone, as compared to group 1 bone (Table 1). Moreover, it was interesting to note that for group 4, bone mineral content increases, as compared to group 3 (Table 1). In the case of group 1 bone, the mean value of the mineral-to-matrix ratio was found to be 2.43 (Figure 5). For group 2 bone, the mean value of the mineral-to-matrix ratio was found to be 2.20. The mineral-to-matrix ratio was decreased for group 3 bone, as compared to group 1 bone, and it was found to be 1.42. As compared to group 3 and group 4 bone, the mineral-to-matrix ratio was increased for group 4 bone, and it was found to be 1.85. No changes were noticed in the loss of the carbonate content to 800°C . It was summarized that diabetic bone had a smaller mineral-to-matrix ratio, as compared to normal bone (Figure 6). Similar to earlier statistical analysis, this data

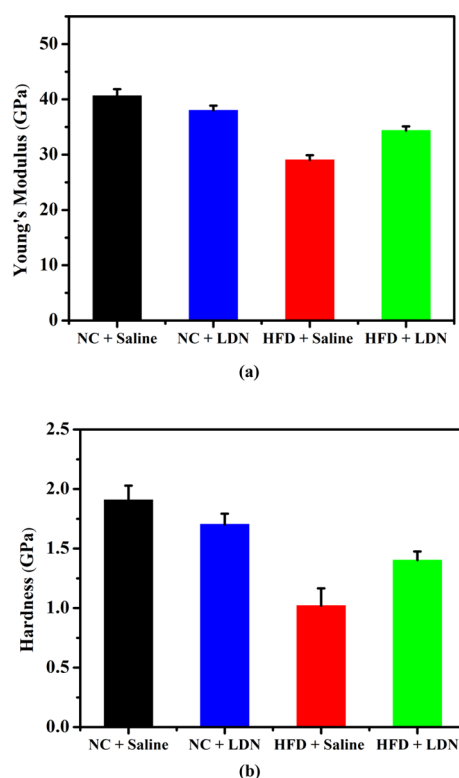


Figure 3. Nano-mechanical properties of different groups of bones; (a) Young's modulus. Two-way ANOVA results indicated a significant effect of diet ($F_{1,20} = 323.16$, $p < 0.001$) and significant interaction between effects of diet and treatment ($F_{1,20} = 87.86$, $p < 0.001$) on Young's modulus; (b) hardness. Two-way ANOVA results indicated a significant effect of diet ($F_{1,20} = 178.7$, $p < 0.001$) and a significant interaction between effects of diet and treatment ($F_{1,20} = 43.7$, $p < 0.001$) on hardness. Bonferroni's post-hoc test showed no significant difference between group 1 and group 2 ($p > 0.05$) and significant difference between group 1 and other two groups ($p < 0.05$). $n = 6/\text{group}$.

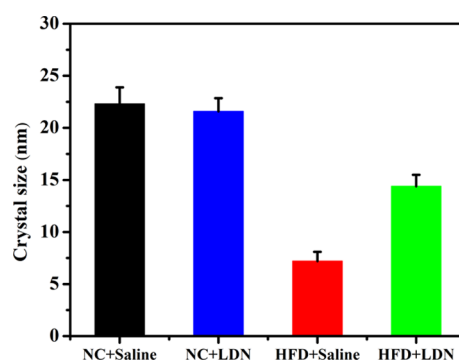


Figure 4. Mineral crystal size of different groups of bones. Two-way ANOVA results showed a significant effect of diet ($F_{1,20} = 1186.67$, $p < 0.001$), and a significant interaction between effects of diet and treatment ($F_{1,20} = 151.62$, $p < 0.001$) was observed. Bonferroni's post-hoc test showed no significant difference between group 1 and group 2 ($p > 0.05$) and significant difference between group 1 and other two groups ($p < 0.05$). $n = 6/\text{group}$.

indicated that diet would deteriorate the bone mineral-to-matrix ratio ($p < 0.05$), whereas the LDN treatment protects this alteration in the T2DM mice bone.

3. DISCUSSION

Nowadays bone property deterioration is a greater concern in diabetic people. There is an immediate need of any suitable candidate which can be labeled as a safe and easily available drug. Naltrexone is already an FDA-approved drug (for opioid addiction); therefore, repurposing the low dose which will be much safer to human is a fruitful option for treating bone-related assault associated with diabetes. This study analyzed the effect of T2DM and LDN on bone fracture and material properties. The present results indicated that T2DM could deteriorate the bone fracture and material properties, whereas the LDN compound can restrict to deteriorate the bone mechanical properties in T2DM bone, which indicated that the LDN compound is "bone-friendly" and has no adverse effect on a normal bone. It has been reported that the hierarchical micro-structure of bone offers resistance at the time of fracture; therefore, it is interesting to study the effect of LDN on bone hierarchy.

For HFD-induced T2DM bone (group 3 bone), the mean value of fracture toughness was found to be $2.21 \text{ MPa m}^{1/2}$, which is 54.5% lower than the normal bone (group 1) (Figure 1), which is well corroborated to earlier published study.⁵ The fracture toughness of group 4 bone was found to be $3.41 \text{ MPa m}^{1/2}$, which indicates that LDN treatment can protect the risk of fracture of bone in T2DM mice (Figure 1). The present study indicated that T2DM could deteriorate the fracture toughness value, whereas the LDN compound can restrict to deteriorate the bone fracture toughness, which indicated that the LDN compound is "bone-friendly" and has no adverse effect on a normal bone. The current study indicated that bone size was increased for T2DM bones, as compared to normal bones, which is well corroborated to earlier clinical observations and experimental investigations by Taylor et al.³¹ and Ionova-Martin et al.⁵ However, values of bone geometric parameters are lower than reported values mentioned by Ionova-Martin et al.⁵ This quantitative mismatch is due to the total bodyweight of mice. Statistical analysis indicated significant influence of diet on bone size ($p < 0.05$), and no significant interaction between the effects of diet and treatment on bone size ($p > 0.05$). The possible reason is due to the serum leptin and serum IGF-I, which cannot be controlled by LDN.⁶ It is generally noted that leptin increases in HFD-induced mice.⁵ These data indicated that LDN can control the fracture toughness; however, it cannot protect to increase the bone size in the T2DM mice group (Figures 1 and 2).

To understand the change in the bone microstructure due to T2DM and LDN treatment, through-wall scanning electron microscopy (SEM) images of the fracture region were studied (Figure 6). Lamellar alignment was observed at the tissue level in the case of the normal control group (Figure 6a). In T2DM condition (group 3), the irregular alignment of osteocyte lacunae and reduction in lamellar alignment at the tissue level (Figure 6c) were noticed. The bone cross-section became porous with a tortuous wall region (Figure 6c). Few straight and most of the wavy lamellar alignments were noticed, and nonsignificant reduction in the alignment of osteocyte lacunae could predict some resistance to irregularity in the alignment of these micro-constituents (Figure 6d) for group 4 bone.

At the mineral level, the average apatite crystal size of diabetic bone along the *c*-axis was reduced. This might be a result of the distorted collagen fibril template in the diabetic

Table 1. Weight Percentage (Mean \pm Standard Deviation) of Organic, Mineral, and Carbonate Contents of Bone Powder of Four Different Groups of Bone Measured Using TGA^a

ingredients	NC + saline	NC + LDN	HFD + saline	HFD + LDN
organic (wt %)	27.5 \pm 1.2	29.35 \pm 1.5	37.02 \pm 1.6	32.40 \pm 0.9
mineral (wt %)	66.8 \pm 1.3	64.70 \pm 1.8	52.41 (\pm 1.7)	60.00 \pm 1.6
carbonate (wt %)	0.24 \pm 0.08	0.44 \pm 0.09	0.99 (\pm 0.1)	0.41 \pm 0.08

^aOrganic (wt %): two-way ANOVA results indicated a significant effect of diet ($F_{1,20} = 133.44$, $p < 0.001$) and interaction between effects of diet and treatment ($F_{1,20} = 35.35$, $p < 0.001$), Bonferroni's post-hoc analysis showed no significant difference between group 1 and group 2 ($p > 0.05$) and significant difference between group 1 and other two groups ($p < 0.05$). Mineral (wt %): two-way ANOVA results indicated a significant effect of diet ($F_{1,20} = 209.42$, $p < 0.001$) and significant interaction between effects of diet and treatment ($F_{1,20} = 53.93$, $p < 0.001$), Bonferroni's post-hoc test showed no significant difference between group 1 and group 2 ($p > 0.05$) and significant difference between group 1 and other two groups ($p < 0.05$). Carbonate (wt %): two-way ANOVA results indicated a significant effect of diet ($F_{1,20} = 93.35$, $p < 0.001$) and significant interaction between effects of diet and treatment ($F_{1,20} = 109.55$, $p < 0.001$), Bonferroni's post-hoc analysis showed a significant difference between group 1 and other groups ($p < 0.05$) and no significant difference between group 2 and group 4 ($p > 0.05$). $n = 6/\text{group}$.

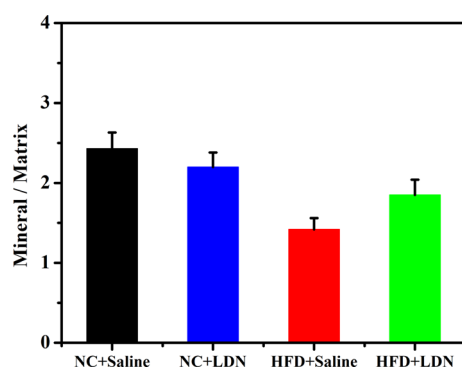


Figure 5. Mineral-to-matrix ratio of different groups of bones. Two-way ANOVA results indicated a significant effect of diet ($F_{1,20} = 119.9$, $p < 0.001$), and a significant interaction between effects of diet and treatment ($F_{1,20} = 28.3$, $p < 0.001$) was observed. Bonferroni's post-hoc test showed no significant difference between group 1 and group 2 ($p > 0.05$) and significant difference between group 1 and other two groups ($p < 0.05$). $n = 6/\text{group}$.

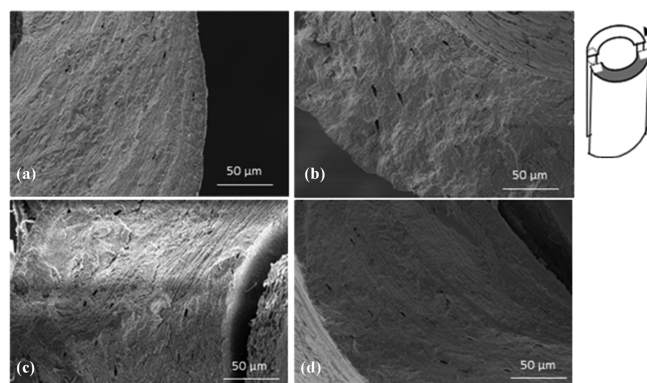


Figure 6. Through-wall SEM images of the fracture region showing tissue structure, (a) (NC + saline): in the case of the normal control group, it shows lamellar alignment at the tissue level, (b) (NC + LDN): no significant changes due to LDN compound treatment on lamellar alignment, (c) (HFD + saline): irregular alignment of osteocyte lacunae and reduction in lamellar alignment at the tissue level due to diabetic obesity, (d) (HFD + LDN): it shows few straight and most of wavy lamellar alignment, nonsignificant reduction in the osteocyte lacunae alignment. The inset shows that images were taken from vertical sections through a region beyond the notch at the crack surface. The dark gray region shows the notch, and the arrow shows the crack growth direction, with propagation of crack happening evenly from both sides of the notch.

bone. It was mentioned in the literature, and transmission electron microscopy and small-angle X-ray scattering measured data have shown that apatite crystals of the brittle *oim*^{-/-} model bone have smaller thickness and packed tightly in a less organized manner, as compared with the normal bone.^{32–34} Additionally, it was reported that smaller crystals have been measured in children with a severe form of *oim*^{-/-}.³⁵ In the current study, it was observed that the difference in mineral crystal size was significant between the brittle diabetic bone and normal control bone; however, T2DM with LDN compound treatment had pronounced resistance to a reduction in the mineral crystal size. It is well mentioned in the literature that variations in the mineral crystal size in bones exhibiting altered mechanical properties occur³⁶ as the mineral crystal size might affect how bone, as a composite material, responds to load.

The bulk mineral content was reduced in diabetic bone, which led to a lower mineral-to-matrix ratio. The moisture content might be affected during sample preparation; therefore, the mineral-to-matrix ratio was calculated using the dry weight at 600 °C. For brittle diseased bone such as *oim*^{-/-}, it was found in the literature that the mineral-to-matrix ratio was increased^{32,37} or decreased.³⁸ These data were measured using Raman spectroscopy and Fourier-transform infrared spectroscopy (FTIR). The inconsistency between Raman, FTIR, and TGA is due to the methodology used to determine the organic and mineral contents. TGA provided a bulk measurement, whereas Raman and FTIR are local measurements. TGA estimates the ratio of the total mineral content (including HA) to the total organic content (including bone matrix collagen, noncollagenous proteins, blood vessels, water molecule, etc.).^{39,40} TGA is complementary to the spectroscopic analyses, indicating that despite the increment in the local phosphate/amide-I ratio found in diabetic bone, there was a decrease in the bulk mineral-to-matrix ratio. A possible reason to increase the total organic fraction in diabetic bone is altered collagen with noncollagenous proteins and blood vessels, which might affect the fracture resistance of bone and other properties.^{41–44}

This study compared the results of mineral and organic contents among normal bone, diabetic bone, and diabetic with LDN treatment bone. In the bone powder sample, lattice water evaporates between 200 and 400 °C, which might contribute to the increased organic weight loss. In diabetic bone samples, water in crystals is lost more easily due to the small size of the crystals and higher surface area. It is also noted that the differences in organic weight loss also increased after 400 °C. Interestingly, organic weight loss is restricted for T2DM with

LDN-treated bone. It was mentioned in the literature that colorimetric measurements of hydroxyproline have measured a decrease in the collagen content in brittle *oim*^{-/-} bone.²³ Therefore, reductions in the collagen content could result in greater mineralization of the bone. There is a scope to find out the influence of LDN on the degree of mineralization of normal and diabetic bones in terms of gray values, instead of translating these values to mineral density using back-scattered electron SEM.

In this study, values of Young's modulus and hardness for normal bone, measured through nano-indentation techniques, are comparable to earlier published data.^{45,46} However, differences were noted when the results were compared with earlier data presented by Rodriguez-Florez et al.⁴⁷ In the present study, the values of Young's modulus and hardness for normal bone were found to be 40.62 and 1.91 GPa, respectively, when bone embedded with dry epoxy. However, Rodriguez-Florez et al.⁴⁷ reported that values were 20.1 and 0.74 GPa, respectively. Results are different, which are due to the selection of indenter size and penetration area. In the present study, the penetration area ($\sim 0.4\text{--}0.6\ \mu\text{m}^2$) was found to be much lower than the penetration area ($\sim 10\text{--}35\ \mu\text{m}^2$) mentioned by Rodriguez-Florez et al.⁴⁷ Therefore, more localized data were obtained in this study than data presented by Rodriguez-Florez et al.⁴⁷ For this reason, the values of Young's modulus and hardness were found to be higher, as compared to data presented by Rodriguez-Florez et al.⁴⁷

This study has a number of limitations. The bone sample was small (six bones per group), and it is quite necessary to repeat these findings using more bones. In macro-level, we have identified only fracture toughness. Including other macro-level properties, such as stiffness, strength, yield strength, and propagation, fracture toughness would be more beneficial for drawing more generalized conclusions related to the effect of LDN on T2DM-affected bone properties.

4. CONCLUSIONS

In this study, the effect of LDN on bone fracture and material properties in HFD-induced T2DM mice bone was investigated. Bone properties were measured in terms of fracture toughness, nano-Young's modulus, hardness, mineral crystal size, bone composition, and bulk mineral to matrix ratio. In the T2DM bone, fracture toughness, nano-Young's modulus, and hardness were decreased, as compared to the normal bone, whereas LDN treatment protects these alterations in T2DM bone. Similar to these, mineral crystal size and mineral-to-matrix ratio were decreased in the HFD-induced T2DM bone, as compared to the normal bone, while treatment with LDN protects these alterations in the T2DM bone. The bone size was increased in the case of HFD-induced T2DM bone; however, LDN cannot protect to increase the bone size in the T2DM bone. The present study concluded that LDN, a TLR4 antagonist treatment, can be used to control the T2DM-affected bone properties at different hierarchical levels.

5. MATERIALS AND METHODS

5.1. Mice Preparation. All experiments were carried out following the guidelines advised by and with the approval of the Animal Ethics Committees of CSIR-IITR, Lucknow, India. Details of the mice preparations and other biological parameters related to T2DM conditions are described in our earlier research paper.⁶ Based on diet and treatment, all mice

were divided into four groups. In group 1 (NC-saline), all mice receive regular chow diet and water ad libitum up to 3 weeks and are subjected to normal saline (i.p) on the fourth and fifth week. In group 2 (NC-LDN), all mice receive regular chow and water ad libitum up to 3 weeks and are subjected to LDN treatment (1 mg/kg bw. i.p) every day for the next 2 weeks (fourth and fifth week). In group 3 (HFD-saline), all mice receive HFD and water ad libitum up to 3 weeks and are subjected to normal saline (i.p) on the fourth and fifth week. In group 4 (HFD-LDN) mice, all mice receive HFD and water ad libitum up to 3 weeks and are subjected to LDN treatment (1 mg/kg bw. i.p) every day for the next 2 weeks (fourth and fifth week).

Right femora (six bones in each group = total 24 bones) were utilized to measure the fracture toughness and bone geometric parameters. Left femora (six bones in each group = total 24 bones) were utilized to measure nano-Young's modulus, hardness, mineral crystal size, and bone composition. Grinding the femur to powder, XRD was used to determine the average apatite mineral crystal size, and TGA was used to differentiate the bulk mineral to matrix ratio. TGA records the loss of bone mass with an increase in temperature from which the fractions of the total mineral content and organic content can be computed. The bulk mineral content of HFD bones and HFD with LDN-treated bones were measured and compared with normal mice bones to measure overall differences at the nano-scale. TGA also measures carbonated mineral and noncollagenous proteins which provide additional intuition to the bulk composition. In this present study, each left femoral bone was cut into two-halves, one-half used for nano-indentation and other half used for XRD and TGA analyses.

5.2. Specimen Preparation and Determination of Bone Fracture Toughness. Right femur bones (six bones in each group = total 24 bones) sample preparation, testing, and determination of fracture toughness were carried out according to the method described by Ritchie et al.⁴⁸ A notch was prepared at the mid-shaft using a low speed saw for all bones. The pre-crack was given with a sharp razor 1 μm diamond suspension at the posterior surface such that total notch and pre-crack were up to $176 \pm 8^\circ$ crack length.⁴⁸ This razor micro-notching technique results in a consistently sharp notch with a root radius of $\sim 10\ \mu\text{m}$. The fracture test was performed at room temperature ($\sim 32\ ^\circ\text{C}$), and all bones were tested using a universal testing machine. After obtaining the breaking load (P), the value of K_{IC} was determined, as per the method described by Ritchie et al.⁴⁸ The value of K_{IC} is given in terms of the wall (bone cortex) thickness t , mean radius R_m of the bone (to the middle of the cortex), and crack length, defined in terms of the half-crack angle θ . The critical stress intensity factor, K_{IC} , was calculated from eq 1

$$K_{\text{IC}} = F_b \sigma_b \sqrt{\pi R_m \theta} \quad (1)$$

where F_b is a geometry factor and σ_b is the applied bending stress which is calculated from the bending moment $M = PS/4$ in terms of the distance from the neutral axis, c , and area moment of inertia I , as $\sigma_b = Mc/I$, and S is the span length.

$$\sigma_b = \frac{M}{2\pi R_m^2 t} \quad (2)$$

Broken half of bones were considered to determine the bone dimensions, such as mean cortical radius, crack angle, and cortical thickness, and these dimensions were measured from

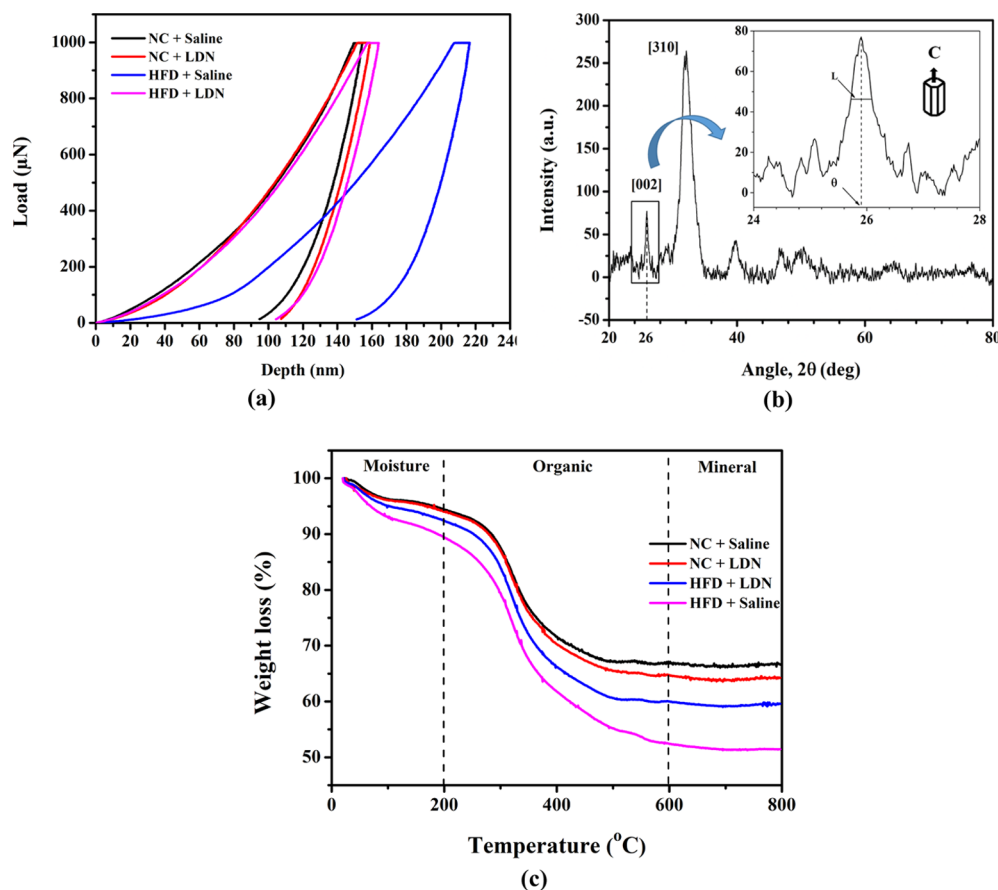


Figure 7. (a) Representative of load-depth curves obtained for different groups of bones by nanoindentation, (b) HA *c*-axis [002] reflections were scanned from 23 to 28° (2θ), and the *a*-axis [310] reflections were scanned from 30 to 44° (2θ). In the case of mineral crystal orientation in bone-powdered samples, the *a*-axis [310] line is not ideally suited to the analysis due to smearing and partial overlapping. However, the peak corresponding to the *c*-axis [002] does not overlap; therefore, this peak at 26° is used to determine the average mineral crystal size in the lattice *c*-direction following eq 6. *L* is full width at half-maximum, and θ is the Bragg angle where the peak is located. (c) Representative TGA curves obtained from different groups of bones heated to 800 °C.

micrographs of the scanning electron microscope.⁴⁸ To find the center of bone cross-section, tangent and its normal were drawn. This process was repeated many times; all normal were passed through a common point, which was considered as a center of the bone cross-section. The mean cortical radius was measured as a distance from the center of the bone cross-section to mid-points between the periosteum and endosteum.⁴⁸ The crack length was measured in terms of crack angle, which is measured from endosteum to endosteum (nearly circular).⁴⁸ Cortical thickness is the distance measured from endosteum to periosteum.⁴⁸ Eight readings were taken for each measurement, and then, the average was taken for the calculation. After obtaining these values, F_b was calculated using the following equations

$$F_b = \left(1 + \frac{t}{2R_m} \right) \left[A_b + B_b \left(\frac{\theta}{\pi} \right) + C_b \left(\frac{\theta}{\pi} \right)^2 + D_b \left(\frac{\theta}{\pi} \right)^3 + E_b \left(\frac{\theta}{\pi} \right)^4 \right] \quad (3)$$

where

$$\begin{aligned} A_b &= 0.65133 - 0.577\xi - 0.3427\xi^2 - 0.0681\xi^3 \\ B_b &= 1.879 + 4.795\xi + 2.343\xi^2 - 0.6197\xi^3 \\ C_b &= -9.779 - 38.14\xi - 6.611\xi^2 + 3.972\xi^3 \\ D_b &= 34.56 + 129.9\xi + 50.55\xi^2 + 3.374\xi^3 \\ E_b &= -30.82 - 147.6\xi - 78.38\xi^2 - 15.54\xi \end{aligned}$$

$$\xi = \log \left(\frac{t}{R_m} \right)$$

We have considered equations of a cylindrical pipe for obtaining these solutions; generally, long bones are not uniform.

5.3. Determination of Bone Size. It is well known that bone size can have an impact on macro-mechanical behavior of cortical bone.⁵ The bone dimensions (or bone size), such as cortical outer radius, cortical inner radius, and cortical thickness, were measured from micrographs of the scanning electron microscope, as discussed in the earlier section.⁴⁸ Once we identified these values, the cross-sectional area and the second moment of area were computed similar to an earlier study.⁵

5.4. Specimen Preparation for Determination of Local Young's Modulus and Hardness of Bone.

The bone shafts were embedded in a mixture having a ratio 4:1 of Epoxy resin (EpoxiCure, Buehler, Lake Bluff, IL, USA) and hardener (EpoxiCure, Buehler, Lake Bluff, IL, USA).⁴⁹ This embedding medium was selected to prevent infiltration of the polymer in the bone porosity, which is considerably limited owing to its high viscosity and fast solidification. In order to expose its cross-section, the molded bones were cut in the transverse direction using a diamond cutter. Ultrapol polishing (Ultratec Manufacturing, Inc.) was used for polishing the bone surface with increasing grades of carbide papers (P400, P600, P1200, and P4000). For cooling the bone surface, water was used. For removal of material, carbide paper P400 and P600 grades were used. Carbide paper P1200 and P4000 grades were used for the final polishing.

5.4.1. Nanoindentation Test. The average surface roughness of the sample of the indentation region was controlled, and only surfaces with the roughness of less than 0.05 μm were considered for indentation.⁵⁰ Nano-indentation tests on the femurs were performed with TI 900 Triboindenter (Hysitron Inc., Minneapolis, MN, USA) with a Berkovich Indenter. A fused silica reference sample was used to calibrate the tip area function and machine compliance by performing 35 indentations between 100 and 10,000 μN maximum load.⁵¹ A ramp-and-hold method was considered, and a maximum load of 1000 μN was applied to determine Young's modulus and hardness. In order to measure data, a loading and unloading rate of 300 and 900 $\mu\text{N s}^{-1}$ and holding time of 30 s at maximum load were chosen similar to the earlier studies.^{10,51} It has been reported that the 30 s holding time was acquired to eliminate the effects of creep.⁵² For each sample, a total of four different locations were considered, and for each location, six indentations were performed on the cross-sectional area of the cortical bone surface. An optical calibration was performed on an aluminum reference sample at the beginning of each set, to ensure the correct tip positioning on the sample. Indentations were located in the middle portion of the cortical bone surface at an approximately equal distance from the periosteum and the endosteum boundaries. The imprint area was approximately 0.6 μm^2 , which corresponds to a contact depth of about 200 nm.⁵³ Hence, each indent was placed 10 μm apart, and no overlap between indents occurred.

The Oliver–Pharr method⁵⁴ was followed to determine the reduced Young's modulus and hardness of the bone from the unloading branch of the load–depth indentation curve (Figure 7a). This method believes that the unloading part of the load–displacement graph is linear elastic. Following equation was used to determine the reduced Young's modulus (E_r)

$$E_r = \frac{1}{\beta} \frac{S\sqrt{\pi}}{2\sqrt{A}} \quad (4)$$

where S is noted as the elastic contact stiffness, β is the geometrical parameter, and A is the area of contact. The value for S was determined similar to the earlier published study.¹⁰ Bone hardness (H) was identified using the following equation by the ratio of the maximum load (P_{max}) to the contact area (A)

$$H = \frac{P_{\text{max}}}{A} \quad (5)$$

where P_{max} is the maximum load and A is the contact area. Load–displacement plots for different groups of bones are shown in Figure 7a.

5.5. XRD of Bone Powder. Soft tissues and bone marrow were removed, and both epiphyses were cut off with a water-cooled low-speed diamond saw (Minitom, Struers, Denmark). Mortar and pestle were used to ground the bones into homogeneous powder. The same femur powder of different groups of bones was used for the XRD and TGA analyses. XRD patterns were obtained using a powder X-ray diffractometer (SmartLab, Rigaku, Japan) operated at 45 kV and 200 mA with Cu $K\alpha$ and radiation wavelength of $\lambda = 1.5406 \text{ \AA}$. Diffractograms were taken from 20 to 80° in a 2θ scale and 0.02° step size for phase identification along with a count time at each step of 35 s. The scanning rate of the test was 2°/min. The diffraction peak at $2\theta = 26^\circ$ was relative to the (0 0 2) c -axis which does not coincide; therefore, it was used to estimate the average crystal size along the c -axis (Figure 7b).^{23,55} The full width at half-maximum method with the Scherrer equation²³ was used to calculate the mineral crystal size

$$B = \frac{k\lambda}{L \cos \theta} \quad (6)$$

Where B is the mineral crystal size, k is the shape factor, λ is the wavelength of the X-ray, L is the peak width at half maximum, and θ is the Bragg angle at the peak. The mean crystal size of all samples was calculated by using this equation.

5.6. TGA with Differential Scanning Calorimetry. TGA was conducted on the Netzsch STA449F1 Jupiter synchronous thermal analyzer. Each test was carried out at a constant heating rate of 10 °C/min in a controlled oxygen atmosphere. 2.5–3 mg of femur bone powder of each sample was heated to the required temperature in an alumina crucible. The change in mass of the bone sample monitored by TGA DSC was noted to be the result of the loss of water for temperature up to 200 °C, organic content from 200 to 600 °C, and carbonate content above 600 °C.^{56–58} All samples were heated from room temperature to 800 °C (Figure 7c). Furthermore, mineral-to-matrix ratio was calculated as the ratio of the percentage of mineral mass remaining after heating to 600 °C and the organic mass loss between 200 and 600 °C (Figure 7c).⁵⁷

$$\frac{\text{mineral}}{\text{matrix}} = \frac{m_{600\text{ }^\circ\text{C}}(\%)}{m_{200\text{ }^\circ\text{C}}(\%) - m_{600\text{ }^\circ\text{C}}(\%)} \quad (7)$$

The mineral mass percentage at 600 °C depends on the amount of moisture mass loss, which might be different in diabetic bones. To overcome this effect, the mass percentage at 600 °C was converted to dry weight percentage for the estimation of the mineral-to-matrix ratio.^{23,56,57}

$$m_{600\text{ }^\circ\text{C}}(\% \text{ dry weight}) = \frac{m_{600\text{ }^\circ\text{C}}(\% \text{ initial weight})}{m_{200\text{ }^\circ\text{C}}(\% \text{ initial weight})} \times 100 \quad (8)$$

TGA curves of weight loss with the temperature of different groups of bone are plotted in Figure 7c.

5.7. Statistical Analysis. Statistical significance test was carried out using two-way ANOVA ($2 \times 2 = 4$ conditions = four different groups of bone) with main effects being diets (normal and HFD) and treatments (saline and LDN) followed by Bonferroni's post-hoc test. Here, output parameters are

controlled by the type of diet and type of treatment; for this reason, two-way ANOVA test for statistical analysis was considered. SPSS (version 19.0) software was used for all statistical analysis. *P*-values less than 0.05 were considered as statistically significant. Data are presented in terms of mean \pm standard deviation.

AUTHOR INFORMATION

Corresponding Authors

Prosenjit Mondal – School of Basic Science, Indian Institute of Technology Mandi, Mandi 175005 Himachal Pradesh, India; Phone: +91 1905267262; Email: prosenjit@iitmandi.ac.in

Rajesh Ghosh – School of Engineering, Indian Institute of Technology Mandi, Mandi 175005 Himachal Pradesh, India; orcid.org/0000-0003-1842-8171; Phone: + 91 1905267903; Email: rajesh@iitmandi.ac.in

Authors

Pankaj Shitole – School of Engineering, Indian Institute of Technology Mandi, Mandi 175005 Himachal Pradesh, India
Abhinav Choubey – School of Basic Science, Indian Institute of Technology Mandi, Mandi 175005 Himachal Pradesh, India

Complete contact information is available at:

<https://pubs.acs.org/10.1021/acsomega.1c02371>

Author Contributions

The manuscript was written through contributions of all authors. All authors have given approval to the final version of the manuscript.

Notes

The authors declare no competing financial interest.

ACKNOWLEDGMENTS

The authors thanks the Director, IIT Mandi for supporting this study. The authors would like to thank IIT Mandi, India for financial support for this work through SEED grant project no. IITM/SG/RG/59. The authors thanks the AMRC and BioX center at IIT Mandi for specimen preparation and scanning electron microscopic images. The authors thanks Davinder Singh and Divya Verma for help during nanoindentation testing. The authors thanks Dr. Debabrata Ghosh and Aditya K Kar (CSIR-IITR) for their help with animal studies and Isita Nandi for her help during the operation of TGA. The authors also express their gratitude toward Puneet Sood for his help while XRD testing.

REFERENCES

- (1) Marshall, J. A.; Bessesen, D. H. Dietary fat and the development of type 2 diabetes. *Diabet. Care* **2002**, *25*, 620–622.
- (2) Jackuliak, P.; Payer, J. Osteoporosis, fractures, and diabetes. *Int. J. Endocrinol.* **2014**, *2014*, 1–10.
- (3) WHO. *WHO Technical Report Series. Diet, Nutrition, and the Prevention of Chronic Diseases: Report of a Joint WHO/FAO Expert Consultation*, Google Books, 2003 (accessed January 25, 2020).
- (4) Knowler, W. C.; Barrett-Connor, E.; Fowler, S. E.; Hamman, R. F.; Lachin, J. M.; Walker, E. A.; Nathan, D. M. Reduction in the incidence of type 2 diabetes with lifestyle intervention or metformin. *N. Engl. J. Med.* **2002**, *346*, 393–403.
- (5) Ionova-Martin, S. S.; Do, S. H.; Barth, H. D.; Szadkowska, M.; Porter, A. E.; Ager, J. W.; Ager, J. W.; Alliston, T.; Vaisse, C.; Ritchie, R. O. Reduced size-independent mechanical properties of cortical bone in high-fat diet-induced obesity. *Bone* **2010**, *46*, 217–225.

- (6) Choubey, A.; Girdhar, K.; Kar, A. K.; Kushwaha, S.; Yadav, M. K.; Ghosh, D.; Mondal, P. Low-dose naltrexone rescues inflammation and insulin resistance associated with hyperinsulinemia. *J. Biol. Chem.* **2020**, *295*, 16359–16369.

- (7) Hutchinson, M. R.; Zhang, Y.; Brown, K.; Coats, B. D.; Shridhar, M.; Sholar, P. W.; Patel, S. J.; Crysdale, N. Y.; Harrison, J. A.; Maier, S. F.; Rice, K. C.; Watkins, L. R. Non-stereoselective reversal of neuropathic pain by naloxone and naltrexone: Involvement of toll-like receptor 4 (TLR4). *Eur. J. Neurosci.* **2008**, *28*, 20–29.

- (8) Cant, R.; Dalgleish, A. G.; Allen, R. L. Naltrexone inhibits IL-6 and TNF α production in human immune cell subsets following stimulation with ligands for intracellular toll-like receptors. *Front. Immunol.* **2017**, *8*, 809.

- (9) Wang, X.; Zhang, Y.; Peng, Y.; Hutchinson, M. R.; Rice, K. C.; Yin, H.; Watkins, L. R. Pharmacological characterization of the opioid inactive isomers (+)-naltrexone and (+)-naloxone as antagonists of toll-like receptor 4. *Br. J. Pharmacol.* **2016**, *173*, 856–869.

- (10) Shitole, P.; Choubey, A.; Mondal, P.; Ghosh, R. Influence of low dose naltrexone on Raman assisted bone quality, skeletal advanced glycation end-products and nano-mechanical properties in type 2 diabetic mice bone. *Mater. Sci. Eng., C* **2021**, *123*, 112011.

- (11) Rosen, C. J.; Bouxsein, M. L. Mechanisms of disease: Is osteoporosis the obesity of bone? *Nat. Clin. Pract. Rheumatol.* **2006**, *2*, 35–43.

- (12) Kanis, J. A. Osteoporosis III: Diagnosis of osteoporosis and assessment of fracture risk. *Lancet* **2002**, *359*, 1929–1936.

- (13) Dimitri, P.; Bishop, N.; Walsh, J. S.; Eastell, R. Obesity is a risk factor for fracture in children but is protective against fracture in adults: A paradox. *Bone* **2012**, *50*, 457–466.

- (14) Brahmabhatt, V.; Rho, J.; Bernardis, L.; Gillespie, R.; Ziv, I. The effects of dietary-induced obesity on the biomechanical properties of femora in male rats. *Int. J. Obes.* **1998**, *22*, 813–818.

- (15) Bahrambeigi, S.; Yousefi, B.; Rahimi, M.; Shafiei-Irannejad, V. Metformin; an old antidiabetic drug with new potentials in bone disorders. *Biomed. Pharmacother.* **2019**, *109*, 1593–1601.

- (16) Rho, J.-Y.; Kuhn-Spearing, L.; Zioupos, P. Mechanical properties and the hierarchical structure of bone. *Med. Eng. Phys.* **1998**, *20*, 92–102.

- (17) Ritchie, R. O.; Nalla, R. K.; Krucic, J. J.; Ager, J. W.; Balooch, G.; Kinney, J. H. Fracture and Ageing in Bone: Toughness and Structural Characterization. *Strain* **2006**, *42*, 225–232.

- (18) Ritchie, R. O.; Buehler, M. J.; Hansma, P. Plasticity and toughness in bone. *Phys. Today* **2009**, *62*, 41–47.

- (19) Fratzl, P.; Gupta, H. S.; Paschalis, E. P.; Roschger, P. Structure and mechanical quality of the collagen-mineral nano-composite in bone. *J. Mater. Chem.* **2004**, *14*, 2115–2123.

- (20) Zimmermann, E. A.; Schaible, E.; Bale, H.; Barth, H. D.; Tang, S. Y.; Reichert, P.; Busse, B.; Alliston, T.; Ager, J. W.; Ritchie, R. O. Age-related changes in the plasticity and toughness of human cortical bone at multiple length scales. *Proc. Natl. Acad. Sci. U.S.A.* **2011**, *108*, 14416–14421.

- (21) Camacho, N. P.; Landis, W. J.; Boskey, A. L. Mineral changes in a mouse model of osteogenesis imperfecta detected by Fourier transform infrared microscopy. *Connect. Tissue Res.* **1996**, *35*, 259–265.

- (22) Tadano, S.; Giri, B. X-ray diffraction as a promising tool to characterize bone nanocomposites. *Sci. Technol. Adv. Mater.* **2011**, *12*, 064708.

- (23) Rodriguez-Florez, N.; Garcia-Tunon, E.; Mukadam, Q.; Saiz, E.; Oldknow, K. J.; Farquharson, C.; Millán, J. L.; Boyde, A.; Shefelbine, S. J. An Investigation of the Mineral in Ductile and Brittle Cortical Mouse Bone. *J. Bone Miner. Res.* **2015**, *30*, 786.

- (24) de Jong, W. F. The mineral substance in the bones. *Collect. Chem.* **1976**, *98*, 445–448.

- (25) Bonar, L. C.; Roufosse, A. H.; Sabine, W. K.; Grynypas, M. D.; Glimcher, M. J. X-ray diffraction studies of the crystallinity of bone mineral in newly synthesized and density fractionated bone. *Calcif. Tissue Int.* **1983**, *35*, 202–209.

- (26) Fantner, G. E.; Birkedal, H.; Kindt, J. H.; Hassenkam, T.; Weaver, J. C.; Cutroni, J. A.; Bosma, B. L.; Bawazer, L.; Finch, M. M.; Cidade, G. A. G.; Morse, D. E.; Stucky, G. D.; Hansma, P. K. Influence of the degradation of the organic matrix on the microscopic fracture behavior of trabecular bone. *Bone* **2004**, *35*, 1013–1022.
- (27) Titunick, M. B.; Lewis, G. S.; Cain, J. D.; Zagon, I. S.; McLaughlin, P. J. Blockade of the OGF-OGFr pathway in diabetic bone. *Connect. Tissue Res.* **2019**, *60*, 521–529.
- (28) Thakur, N. A.; DeBoyace, S. D.; Margulies, B. S. Antagonism of the Met5-enkephalin-opioid growth factor receptor-signaling axis promotes MSC to differentiate into osteoblasts. *J. Orthop. Res.* **2016**, *34*, 1195–1205.
- (29) Tanaka, K.; Kondo, H.; Hamamura, K.; Togari, A. Systemic administration of low-dose naltrexone increases bone mass due to blockade of opioid growth factor receptor signaling in mice osteoblasts. *Life Sci.* **2019**, *224*, 232–240.
- (30) Doustimotlagha, A. H.; Dehpourb, A. R.; Etemad-Moghadam, S.; Alaeddinic, M.; Kheirandishd, Y.; Golestania, A. Effect of Naltrexone and L-NAME on bone densitometry in bile duct ligated rats. *8th International Congress of Laboratory and Clinic*: Tehran, Iran, 6–8 February 2016.
- (31) Taylor, E. D.; Theim, K. R.; Mirch, M. C.; Ghorbani, S.; Tanofsky-Kraff, M.; Adler-Wailes, D. C.; Brady, S.; Reynolds, J. C.; Calis, K. A.; Yanovski, J. A. Orthopedic complications of overweight in children and adolescents. *Pediatrics* **2006**, *117*, 2167–2174.
- (32) Vanleene, M.; Porter, A.; Guillot, P.-V.; Boyde, A.; Oyen, M.; Shefelbine, S. Ultra-structural defects cause low bone matrix stiffness despite high mineralization in osteogenesis imperfecta mice. *Bone* **2012**, *50*, 1317–1323.
- (33) Grabner, B.; Landis, W. J.; Roschger, P.; Rinnerthaler, S.; Peterlik, H.; Klaushofer, K.; Fratzl, P. Age- and genotype-dependence of bone material properties in the osteogenesis imperfecta murine model (oim). *Bone* **2001**, *29*, 453–457.
- (34) Fratzl, P.; Paris, O.; Klaushofer, K.; Landis, W. J. Bone mineralization in an osteogenesis imperfecta mouse model studied by small-angle x-ray scattering. *J. Clin. Invest.* **1996**, *97*, 396–402.
- (35) Vetter, U.; Eanes, E. D.; Kopp, J. B.; Termine, J. D.; Robey, P. G. Changes in apatite crystal size in bones of patients with osteogenesis imperfecta. *Calcif. Tissue Int.* **1991**, *49*, 248–250.
- (36) Boskey, A. L. Bone mineral crystal size. *Osteoporos. Int.* **2003**, *14*, 16–21.
- (37) Carriero, A.; Zimmermann, E. A.; Paluszny, A.; Tang, S. Y.; Bale, H.; Busse, B.; Alliston, T.; Kazakia, G.; Ritchie, R. O.; Shefelbine, S. J. How tough is brittle bone? Investigating osteogenesis imperfecta in mouse bone. *J. Bone Miner. Res.* **2014**, *29*, 1392–1401.
- (38) Bart, Z. R.; Hammond, M. A.; Wallace, J. M. Multi-scale analysis of bone chemistry, morphology and mechanics in the oim model of osteogenesis imperfecta. *Connect. Tiss. Res.* **2014**, *55*, 4–8.
- (39) Pramanik, S.; Hanif, A.; Pingguan-Murphy, B.; Abu Osman, N. Morphological change of heat treated bovine bone: A comparative study. *Materials* **2012**, *6*, 65–75.
- (40) Wang, X.-Y.; Zuo, Y.; Huang, D.; Hou, X.-D.; Li, Y.-B. Comparative study on inorganic composition and crystallographic properties of cortical and cancellous bone. *Biomed. Environ. Sci.* **2010**, *23*, 473–480.
- (41) Miller, E.; Delos, D.; Baldini, T.; Wright, T. M.; Pleshko Camacho, N. Abnormal mineral-matrix interactions are a significant contributor to fragility in oim/oim bone. *Calcif. Tissue Int.* **2007**, *81*, 206–214.
- (42) Buehler, M. J. Nanomechanics of collagen fibrils under varying cross-link densities: Atomistic and continuum studies. *J. Mech. Behav. Biomed. Mater.* **2008**, *1*, 59–67.
- (43) Tang, S. Y.; Vashishth, D. The relative contributions of non-enzymatic glycation and cortical porosity on the fracture toughness of aging bone. *J. Biomech.* **2011**, *44*, 330.
- (44) Abdel-Wahab, A. A.; Maligno, A. R.; Silberschmidt, V. V. Micro-scale modelling of bovine cortical bone fracture: Analysis of crack propagation and microstructure using X-FEM. *Comput. Mater. Sci.* **2012**, *52*, 128–135.
- (45) Middleton, K. M.; Goldstein, B. D.; Guduru, P. R.; Waters, J. F.; Kelly, S. A.; Swartz, S. M.; Garland, T. Variation in within-bone stiffness measured by nanoindentation in mice bred for high levels of voluntary wheel running. *J. Anat.* **2010**, *216*, 121–131.
- (46) Miller, L. M.; Little, W.; Schirmer, A.; Sheik, F.; Busa, B.; Judex, S. Accretion of Bone Quantity and Quality in the Developing Mouse Skeleton. *J. Bone Miner. Res.* **2007**, *22*, 1037–1045.
- (47) Rodriguez-Florez, N.; Oyen, M. L.; Shefelbine, S. J. Insight into differences in nanoindentation properties of bone. *J. Mech. Behav. Biomed. Mater.* **2013**, *18*, 90–99.
- (48) Ritchie, R. O.; Koester, K. J.; Ionova, S.; Yao, W.; Lane, N. E.; Ager, J. W. Measurement of the toughness of bone: A tutorial with special reference to small animal studies. *Bone* **2008**, *43*, 798–812.
- (49) Casanova, M.; Balmelli, A.; Carnelli, D.; Courty, D.; Schneider, P.; Müller, R. Nanoindentation analysis of the micromechanical anisotropy in mouse cortical bone. *R. Soc. Open Sci.* **2017**, *4*, 160971.
- (50) Fischer-Cripps, A.; Nicholson, D. Nanoindentation, Mechanical Engineering Series. *Appl. Mech. Rev.* **2004**, *57*, B12.
- (51) Oliver, W. C.; Pharr, G. M. Measurement of hardness and elastic modulus by instrumented indentation: Advances in understanding and refinements to methodology. *J. Mater. Res.* **2004**, *19*, 3–20.
- (52) Fan, Z.; Rho, J.-Y. Effects of viscoelasticity and time-dependent plasticity on nanoindentation measurements of human cortical bone. *J. Biomed. Mater. Res., Part A* **2003**, *67*, 208–214.
- (53) Lucchini, R.; Carnelli, D.; Ponzoni, M.; Bertarelli, E.; Gastaldi, D.; Vena, P. Role of damage mechanics in nanoindentation of lamellar bone at multiple sizes: Experiments and numerical modeling. *J. Mech. Behav. Biomed. Mater.* **2011**, *4*, 1852–1863.
- (54) Oliver, W. C.; Pharr, G. M. An improved technique for determining hardness and elastic modulus using load and displacement sensing indentation experiments. *J. Mater. Res.* **1992**, *7*, 1564–1583.
- (55) Boskey, A. L.; Moore, D. J.; Amling, M.; Canalis, E.; Delany, A. M. Infrared Analysis of the Mineral and Matrix in Bones of Osteonectin-Null Mice and Their Wildtype Controls. *J. Bone Miner. Res.* **2003**, *18*, 1005–1011.
- (56) Legros, R.; Balmain, N.; Bonel, G. Age-related changes in mineral of rat and bovine cortical bone. *Calcif. Tissue Int.* **1987**, *41*, 137–144.
- (57) Peters, F.; Schwarz, K.; Epple, M. The structure of bone studied with synchrotron X-ray diffraction, X-ray absorption spectroscopy and thermal analysis. *Thermochim. Acta* **2000**, *361*, 131–138.
- (58) Wang, X.-M.; Cui, F.-Z.; Ge, J.; Ma, C. Alterations in mineral properties of zebrafish skeletal bone induced by liliputdct232 gene mutation. *J. Cryst. Growth* **2003**, *258*, 394–401.